nature energy

ARTICLES

https://doi.org/10.1038/s41560-018-0232-y

Bias-free photoelectrochemical water splitting with photosystem II on a dye-sensitized photoanode wired to hydrogenase

Katarzyna P. Sokol[1], William E. Robinson[1], Julien Warnan[1], Nikolay Kornienko[1], Marc M. Nowaczyk[2], Adrian Ruff[3], Jenny Z. Zhang[1] and Erwin Reisner[1]*

Natural photosynthesis stores sunlight in chemical energy carriers, but it has not evolved for the efficient synthesis of fuels, such as H_2. Semi-artificial photosynthesis combines the strengths of natural photosynthesis with synthetic chemistry and materials science to develop model systems that overcome nature's limitations, such as low-yielding metabolic pathways and non-complementary light absorption by photosystems I and II. Here, we report a bias-free semi-artificial tandem platform that wires photosystem II to hydrogenase for overall water splitting. This photoelectrochemical cell integrated the red and blue light-absorber photosystem II with a green light-absorbing diketopyrrolopyrrole dye-sensitized TiO_2 photoanode, and so enabled complementary panchromatic solar light absorption. Effective electronic communication at the enzyme–material interface was engineered using an osmium-complex-modified redox polymer on a hierarchically structured TiO_2. This system provides a design protocol for bias-free semi-artificial Z schemes in vitro and provides an extended toolbox of biotic and abiotic components to re-engineer photosynthetic pathways.

Semi-artificial photosynthesis bridges the rapidly progressing fields of synthetic biology and artificial photosynthesis, and offers a platform to develop and understand solar fuel generation[1–4]. Synthetic biology has vastly opened up the way that nature can be manipulated to streamline functionality and to build artificial biological systems, but its complex machineries and metabolic pathways limit engineering flexibility[5]. Artificial photosynthesis utilizes synthetic, often biomimetic, components to convert and store solar energy, but it is often constrained by inefficient catalysis and costly and/or toxic materials[6]. Semi-artificial photosynthesis aims to integrate the high efficiency and selectivity of enzymes with the controllability of synthetic materials to photocatalyse endergonic reactions in the absence of competing processes[7]. It also allows the construction of biologically inaccessible pathways with a high level of control and flexibility[3]. The catalytic activity of redox enzymes can be harnessed when adsorbed on electrodes by protein film electrochemistry and protein film photoelectrochemistry (PF-PEC)[8,9]. A key challenge is to design biotic–abiotic interfaces that effectively wire together the biological and synthetic components to operate at their optimum.

Solar-driven water splitting into H_2 and O_2 is the most prominent model reaction in artificial photosynthesis[10]. Inefficient catalysis (particularly, kinetically slow O_2 evolution and the formation of partially oxidized side products) is a major limitation in synthetic systems, and results in the requirement of large overpotentials and energy conversion losses[6]. Oxygenic organisms convert solar energy using a photosynthetic Z scheme that contains two light absorbers, photosystem I (PSI) and photosystem II (PSII)[11]. In this tandem configuration, the first excitation in PSII drives water oxidation to O_2 and produces a proton gradient, whereas the second excitation in PSI generates a low potential electron to drive CO_2 fixation into sugars[12]. Alternatively, H_2 can be produced from microalgae and cyanobacteria via electron transfer from ferredoxin to a [FeFe]-hydrogenase ([FeFe]-H_2ase), which reduces protons to H_2 (ref. [13]). The efficiencies for photobiological H_2 production are low for several reasons[14,15]. First, PSII and PSI overlap in light absorption and compete for a small fraction of the solar spectrum. Second, high light intensities limit the efficient electron flux upstream and downstream of PSII. Third, in vivo H_2 production relies on O_2-sensitive [FeFe]-H_2ases, which prevents sustained water splitting. Fourth, CO_2 fixation is preferred over proton reduction, which leads to low H_2 yields. Overcoming these limitations offers scope to enhance H_2 production with biological components.

We previously reported a PEC water-splitting system with a PSII photoanode wired to a [NiFeSe]-H_2ase cathode[3]. However, this system relied solely on light absorption by PSII and required an externally applied voltage due to the low electrochemical potential of the electrons that leave PSII. This limitation can be resolved by introducing a second light absorber to further promote the energetics of the electrons to be delivered to H_2ase[16]. To generate sufficient driving force for overall water splitting, while maximizing solar energy harvesting, complementary dual-absorber/tandem systems can be assembled, which show theoretical limits for a solar-to-hydrogen efficiency of up to 25%[17]. PSII[18,19] and $BiVO_4$ (ref. [20]) photoanodes wired to PSI photocathodes have been reported to produce electricity, but no chemical fuel. Tandem systems that contain PSII have not been combined with enzymatic fuel synthesis[21–23].

Here, a semi-artificial system for the unassisted, light-driven water splitting with PSII and H_2ase is presented. This PEC system does not require an external energy input as dual light absorption is realized by a tandem photoanode that consists of PSII wired to dye-sensitized titanium dioxide (TiO_2), which provides a

[1]Department of Chemistry, University of Cambridge, Cambridge, UK. [2]Plant Biochemistry, Faculty of Biology & Biotechnology, Ruhr-Universität Bochum, Bochum, Germany. [3]Analytical Chemistry – Center for Electrochemical Sciences (CES), Faculty of Chemistry and Biochemistry, Ruhr-Universität Bochum, Bochum, Germany. *e-mail: reisner@ch.cam.ac.uk

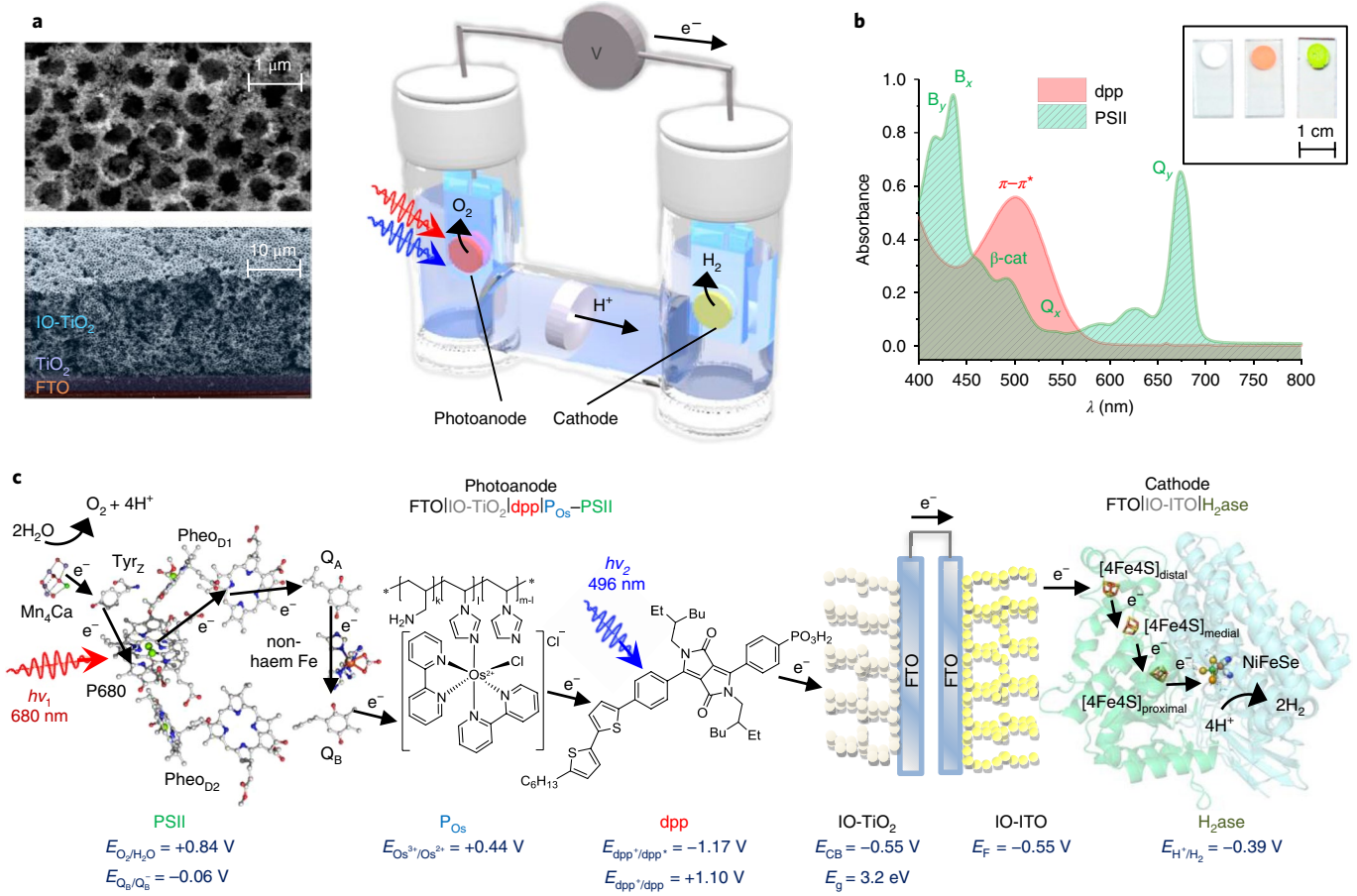

Fig. 1 | Semi-artificial tandem PEC system for unassisted overall water splitting. a, Schematic representation (right) of the PEC cell with IO-TiO_2|dpp|P_{Os}–PSII photoanode wired to the IO-ITO|H_2ase cathode. SEM images (left) of the IO-TiO_2 photoanode architecture (top view (top) and cross-section at a 60° tilt angle (bottom)). **b**, Solution UV–vis spectra of dpp (0.15 μM in THF) and PSII (0.005 mg chlorophyll *a* ml^{-1} in H_2O). Inset: photographic images of IO-TiO_2 (left), IO-TiO_2|dpp (middle) and IO-TiO_2|PSII (right). Absorptions: $B_{y/x}$, chlorophyll *a* Soret bands; β-cat, β-carotene; $Q_{x/y}$, chlorophyll *a* lowest-energy bands; π–π^*, dpp π-orbital intramolecular charge transfer. **c**, Electron-transfer pathway between PSII, P_{Os}, dpp, IO-TiO_2, IO-ITO and H_2ase (species size not drawn to scale) and the relevant redox potentials. Mn_4Ca, oxygen-evolving complex; Tyr_Z, tyrosine; P680, pigment/primary electron donor; Pheo, pheophytin; Q_A/Q_B, plastoquinones; [NiFeSe], H_2ase active site; [4Fe4S], iron sulfur clusters; E_g, bandgap energy; E_F, Fermi energy level; all the potentials are reported versus SHE at pH 6.5. PSII: C, grey; O, red; N, blue; Mn, violet; Ca, green; Mg, light green. H_2ase: S, yellow; Fe, brown; Ni, green; Se, light orange.

sufficient voltage to reduce protons using a H_2ase cathode. This PEC design was inspired by dye-sensitized solar cells[24,25] and it allows PSI to be replaced by a rationally designed diketopyrrolopyrrole (dpp) dye with an absorption complementary to that of PSII. An efficient electronic communication between PSII and dpp was achieved by using the redox polymer poly(1-vinylimidazole-*co*-allylamine)–$Os(bipy)_2Cl$ (P_{Os}), which bypasses possible limitations from an inefficient interfacial electron transfer. Simultaneously, the hydrogel character of the redox polymer provides a solvated environment for the biocatalyst. A hierarchically structured inverse opal TiO_2 (IO-TiO_2) scaffold was employed to provide a high surface area for the effective integration of polymer/PSII.

Assembly of the tandem PSII–dye photoanode

The components and assembly of the PEC tandem cell are depicted in Fig. 1 and the principle of operation as a semi-artificial Z scheme is shown in Supplementary Fig. 1. Hierarchically structured IO-TiO_2 electrodes were assembled on a TiO_2-layer-protected fluorine-doped tin oxide (FTO)-coated glass substrate via a modified co-assembly method (Supplementary Fig. 2)[3]. The TiO_2 protection layer was used to prevent the direct contact of the electroactive components (PSII and P_{Os}) with the FTO. The optimal thickness of the IO-TiO_2 film was determined to be 20 μm, based on preliminary electrochemical screening, and was utilized throughout this work[4]. Scanning electron microscopy (SEM) revealed a diameter of 750 nm for the TiO_2 macropores with connecting channels of 150 nm and a mesoporous skeleton with a porosity of approximately 50 nm. The macroporosity permits the penetration of the bulky PSII and P_{Os} (~20 nm and 16 nm in size, respectively)[3,4], whereas the mesoporous structure provides an enhanced effective surface area for the guest adsorption.

Dye sensitization of the IO-TiO_2 photoanodes (geometrical surface area, $A = 0.25\ cm^2$) was performed by soaking IO-TiO_2 in a tetrahydrofuran (THF) solution of dpp[26,27] overnight (Supplementary Fig. 3). The resulting IO-TiO_2|dpp electrodes had a dpp surface loading of $72 \pm 4\ nmol\ cm^{-2}$ (estimated by spectrophotometry (Supplementary Fig. 4)), consistent with previously reported loadings of molecular species on mesoporous metal oxide scaffolds[28]. The organic dpp dye was selected for its complementary absorption spectrum to PSII and for its ability to act as an efficient visible light photosensitizer for TiO_2 in aqueous media, chemisorbed via its phosphonic acid anchoring group[27]. For comparison, electrodes were also prepared using the ruthenium bis(2,2′-bipy)(4,4′-bis(phosphonic acid)-2,2′-bipy) dibromide dye (RuP; bipy, 2,2′-bipyridine)[29–32], which is commonly used as a benchmark in aqueous dye-sensitized schemes (Supplementary Figs. 1c and 3).

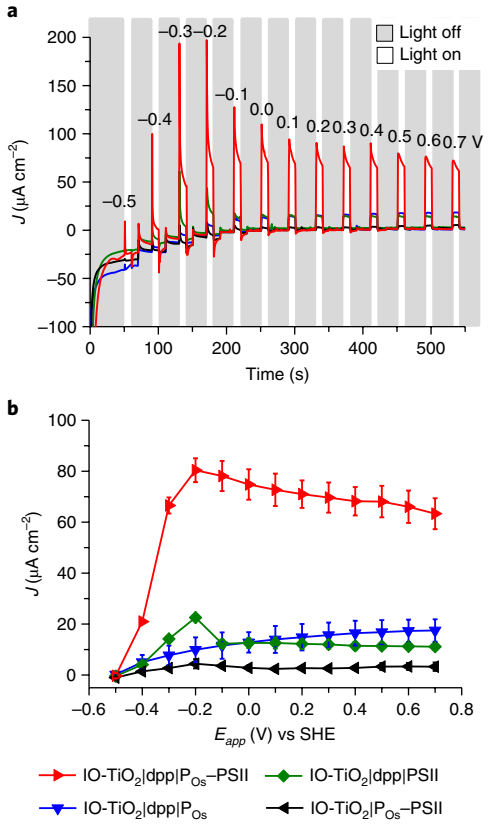

Fig. 2 | PF-PEC of tandem PSII–dye photoanode. a, Chronoamperometry (0.1 V potential steps with 30 s dark and 10 s light cycles) for the determination of the onset potential (E_{onset}) and limiting photocurrent for the IO-TiO_2|dpp|P_{Os}–PSII photoanode. E_{app} values (shown above the peaks) are reported versus SHE. Short irradiation times were used to minimize the PSII photodegradation. **b**, Photocurrent density (J) plotted as a function of E_{app} determined by the stepped potential chronoamperometry in **a**. Values of J were taken at the end of the illumination (baseline corrected for the background dark current). Error bars correspond to the s.d. ($n=3$). Control experiments that omitted one of the components of the tandem photoanode are also presented in **a** and **b**. Conditions: PSII electrolyte solution, pH = 6.5, T = 25 °C. Counter and reference electrodes were a Pt wire and Ag/AgCl (3 M KCl), respectively.

The macroporous voids of the IO-TiO_2|dpp electrodes were subsequently filled with a blend of PSII and P_{Os} to give the fully integrated IO-TiO_2|dpp|P_{os}–PSII tandem photoanode. The PSII chosen for this study was isolated from the thermophilic cyanobacterium *Thermosynechococcus elongatus* as a well characterized[33,34], highly active and relatively robust PSII variant[35,36]. Loadings of 24 ± 4 nmol cm^{-2} and 143 ± 25 pmol cm^{-2} were determined by inductively coupled plasma optical emission spectroscopy (ICP-OES) and Ultraviolet–visible (UV–vis) spectrophotometry for P_{Os} and PSII, respectively (Supplementary Fig. 4). The redox polymer P_{Os} mediates the electron transfer between PSII and the IO-TiO_2|dpp surface, which enhances their electrical connection and physically stabilizes PSII on the electrode[4,37]. The integration of all the biotic and abiotic components in the hybrid photoanode was further confirmed by high angular annular dark field scanning transmission electron microscopy (HAADF–STEM) (Supplementary Fig. 5).

The UV–vis absorption spectra of dpp, P_{Os} and PSII in solution and individually adsorbed on the IO-TiO_2 electrodes were recorded (Fig. 1 and Supplementary Fig. 6). IO-TiO_2|PSII displays absorption maxima (λ_{max}) at 450 nm ($B_{x/y}$ Soret bands) and 680 nm (Q_y band)[38], whereas IO-TiO_2|dpp showed a broad absorption from 475 to 575 nm. Thus, the absorption spectra of the co-sensitized IO-TiO_2 electrode demonstrate a panchromatic light absorption and highlight the light harvester's complementarity desired for a semi-artificial Z scheme. For comparison, the spectrum of RuP (λ_{max} = 457 nm) significantly overlaps with that of PSII (λ_{max} of the $B_{x/y}$ band at 450 nm). The IO-TiO_2|P_{Os} spectrum consisted of a broad and weak absorption, in line with the modest molar absorption of P_{Os} (extinction coefficient $\varepsilon = 8.72\ mM^{-1}\ cm^{-1}$ at 531 nm)[4], which is not expected to substantially affect the light conversion efficiency in the fully assembled IO-TiO_2|dpp|P_{Os}–PSII tandem system.

Photoelectrochemistry

The photocurrent response (J) of IO-TiO_2|dpp|P_{Os}–PSII was recorded by PF-PEC at an applied potential (E_{app}) in a three-electrode configuration. Stepped potential chronoamperometry under a periodic illumination with ultraviolet-filtered simulated solar light was used (1.5 AM filter, light intensity flux (irradiance) $E_e = 100\ mW\ cm^{-2}$, $\lambda > 420$ nm (Fig. 2)). Photogenerated electrons in PSII are transferred to the electron acceptor plastoquinone B (Q_B) (Fig. 1)[9]. The holes are collected at the oxygen-evolving complex, where water is oxidized to liberate protons and gaseous O_2. The conduction band (CB) of IO-TiO_2 receives electrons from the photoexcited dpp which is thereby oxidized (dpp^+) to give rise to an anodic photocurrent. The Os^{3+} complex embedded in P_{Os} mediates the electrons between the reduced Q_B and oxidized dpp to close the electric circuit between the two light absorbers.

The photoanodic current onset potential (E_{onset}) of approximately −0.5 V versus the standard hydrogen electrode (SHE) is consistent with the reported anatase TiO_2 CB edge of approximately −0.6 versus SHE[39] (Fig. 2 and Supplementary Fig. 7). The IO-TiO_2|dpp|P_{Os}–PSII tandem electrode exhibits a shift of more than 0.5 V towards a negative potential compared to single-absorber photoanodes with immobilized PSII[3,4,40], which makes it a promising candidate for bias-free overall water splitting. Potential-independent steady-state photocurrents ($80\ \mu A\ cm^{-2}$) were observed at $E_{app} > -0.2$ V versus SHE (Fig. 2b) and attributed to water oxidation[3,4]. Prolonged irradiation at $E_{app} > -0.2$ V versus SHE results in an irreversible drop in photocurrent, most probably due to PSII photodegradation (irreversible light-induced D1 subunit damage)[4].

Control experiments that omitted one component of the tandem photoanode exhibited only a marginal photoactivity. The small background photoresponse for IO-TiO_2|dpp|PSII and IO-TiO_2|dpp|P_{Os} (Fig. 2), and similarly for IO-TiO_2|dpp (Supplementary Fig. 7a,b) can be assigned to the stoichiometric electron transfer from photoexcited dpp (dpp*) to TiO_2 without the regeneration and photocatalytic turnover of the dye. A low photocurrent in the absence of P_{Os} (IO-TiO_2|dpp|PSII) supports an insufficient direct electronic interaction between PSII and dpp without the redox polymer[4]. No significant photocurrents were observed in the absence of dpp (IO-TiO_2|P_{Os}–PSII (Fig. 2) and IO-TiO_2, IO-TiO_2|P_{Os} and IO-TiO_2|PSII (Supplementary Fig. 7a,b)), consistent with the more positive reduction potentials of PSII's Q_B and P_{Os} relative to the CB of TiO_2, which results in an unfavourable electron transfer. The presented semi-artificial system therefore demonstrates the successful assembly of a functional biotic–abiotic interface for a controlled electron transfer in an artificial Z scheme. A PSII tandem system based on IO-TiO_2|RuP was also assembled and exhibited a similar behaviour (Supplementary Fig. 7c,d). To maximize the performance of the tandem systems, screenings of the dye loading (Supplementary Fig. 8), P_{Os}–PSII ratio (Supplementary Fig. 9) and IO-TiO_2 thickness (Supplementary Fig. 10) were conducted.

Photocurrent action spectrum

The photocurrent response as a function of irradiation wavelength (the photocurrent action spectrum) was recorded for

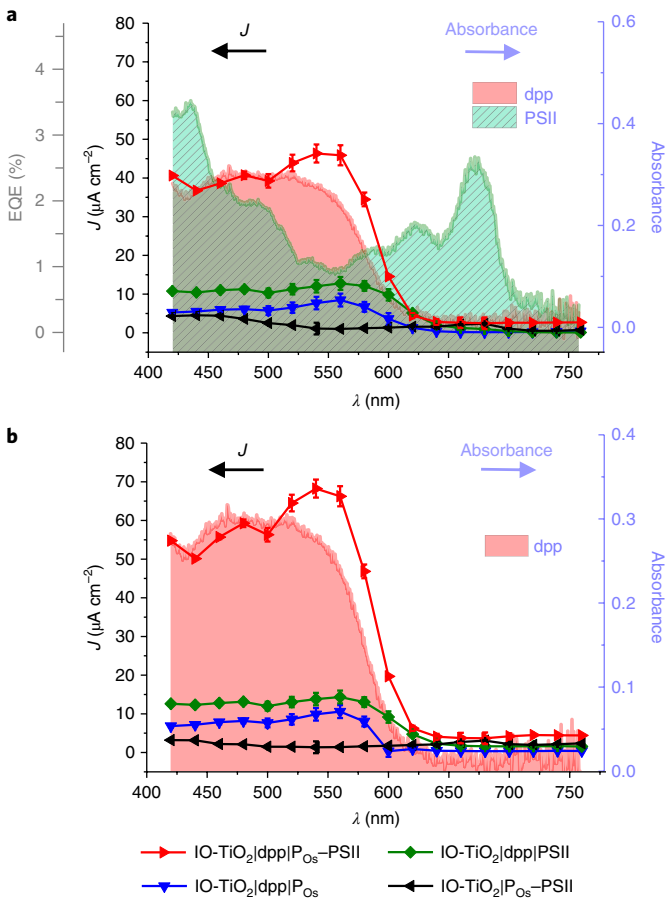

Fig. 3 | Photocurrent action spectra of tandem PSII–dye photoanode. **a**, Single-wavelength action spectra of the IO-TiO_2|dpp|P_{Os}–PSII recorded with monochromatic light (λ_{scan}) measured in 20 nm steps from 760 to 420 nm (E_e = 6 mW cm^{-2}). The grey *y* axis (left) shows the corresponding external quantum efficiency (EQE) values. **b**, Dual-wavelength action spectra recorded with monochromatic light (λ_{scan}) measured in 20 nm steps from 760 to 420 nm (E_e = 6 mW cm^{-2}) and a second simultaneous irradiation at a constant wavelength (λ_{const}) = 660 nm (E_e = 4 mW cm^{-2}). The action spectra were normalized to equal the photon flux at 500 nm (0.26 mmol m^{-2} s^{-1}). The control experiments (with the IO-TiO_2|dpp|PSII, IO-TiO_2|dpp|P_{Os} and IO-TiO_2|P_{Os}–PSII photoanodes) are also given. The right *y* axis (blue) refers to the UV-vis spectra of the background-corrected dpp (72 nmol cm^{-2}) and PSII (155 pmol cm^{-2}) immobilized on the IO-TiO_2 electrodes (shaded in red and turquoise in the background). Conditions for all experiments: PSII electrolyte solution, pH = 6.5, T = 25 °C, E_{app} = 0.5 V versus SHE. The error bars correspond to the s.d. (n = 3).

IO-TiO_2|dye|P_{Os}–PSII and relevant control samples (Fig. 3a) to characterize the complementary light absorption of the tandem photoanode (Supplementary Fig. 1). In a typical experiment, the wavelength was decreased from 760 to 420 nm (λ_{scan}) at E_{app} = 0.5 V versus SHE while measuring the photocurrent. The action spectra were corrected to equal the photon flux at each wavelength and normalized (Supplementary Figs. 11 and 12).

In agreement with the photocurrent responses under full visible light irradiation (Fig. 2), IO-TiO_2, IO-TiO_2|P_{Os}, IO-TiO_2|PSII and IO-TiO_2|P_{Os}–PSII gave negligible photocurrents on monochromatic light illumination across all wavelengths (Fig. 3a). PSII-free electrodes loaded with dpp (IO-TiO_2|dpp, IO-TiO_2|dpp|P_{Os}) gave small photocurrent responses concurrent with the absorption spectrum of dpp, consistent with the assignment of background current due to dpp photooxidation (see above). For the functional IO-TiO_2|dpp|P_{Os}–PSII tandem system, the photocurrent onset was observed at λ_{scan} = 620 nm, with a maximum photocurrent at approximately 560 nm. This photoresponse is consistent with the spectral overlap of PSII with dpp and the required simultaneous excitation of both photoactive components[41]. The absence of photocurrent at λ_{scan} > 620 nm is consistent with the requirement of dpp excitation for the electron injection into the CB of TiO_2 and for P_{Os} oxidation. An external quantum efficiency[21] of 2.7% was obtained at λ_{max} = 560 nm (E_e = 6 mW cm^{-2}).

Dual-wavelength action spectra were also recorded by coupling excitation by the scanned monochromatic light (λ_{scan}) to simultaneous irradiation at a fixed wavelength to continuously excite either PSII (λ_{const} = 660 nm (Fig. 3b and Supplementary Fig. 12b)) or dpp (λ_{const} = 523 nm (Supplementary Fig. 12c)). Continuous excitation of PSII (thereby probing dpp) in IO-TiO_2|dpp|P_{Os}–PSII (Fig. 3b) led to an action spectrum profile (with regard to λ_{scan}) similar to the UV–vis spectrum of dpp and the single-wavelength excitation experiment. In comparison to the latter, a maximum at λ_{scan} = 550 nm was also observed, but with a 40% higher photocurrent magnitude. The overall photocurrent cross-section using dual excitation (Fig. 3b) was approximately two times higher compared to the cross-sections of individual components (Fig. 3a), which confirms the functional and efficient dual-absorber tandem mechanism in IO-TiO_2|dpp|P_{Os}–PSII (Supplementary Fig. 1).

Continuous excitation of dpp (which probes PSII) (Supplementary Fig. 12c) resulted in a general increase in the photocurrent across all wavelengths (760–420 nm) compared to the single-wavelength excitation action spectrum. A new photocurrent maximum was detected at 680 nm, which corresponds to the PSII Q_y band. A photocurrent maximum at 550 nm remained, which corresponded to the higher intensity excitation of the PSII/dpp spectral overlap region and led to a higher photocurrent compared to the single-wavelength experiment. Absorption at 480 nm, which corresponded to the excitation of the PSII β-carotene, and at ≤420 nm, which corresponded to the excitation of the B_x and B_y bands, were also observed. Action spectra of the RuP-sensitized photoanodes recorded for comparison (Supplementary Figs. 13 and 14) also correlated with the UV–vis absorption spectrum of RuP (Supplementary Fig. 6) and exhibited analogous features.

Bias-free overall water splitting via an artificial Z scheme

The negative E_{onset} and broad absorption spectrum of the IO-TiO_2|dpp|P_{Os}–PSII tandem photoanode make it a suitable light absorber for bias-free (unassisted) overall water splitting. To achieve this long-standing goal[16,42], the photoanode was wired to a previously reported indium tin oxide (ITO)-based IO-ITO|H_2ase cathode[3], which utilizes a reversible biological electrocatalyst for H_2 production integrated in a hierarchically structured ITO electrode. The *Desulfomicrobium baculatum* [NiFeSe]-H_2ase was used for its high proton reduction activity, O_2 tolerance under reductive conditions and marginal inhibition by H_2, which offer advantageous properties for water splitting compared to the O_2-sensitive [FeFe]-H_2ases available in algal H_2 production[43]. ITO has been shown to be a suitable electrode material for the wiring of [NiFeSe]-H_2ases in a direct electron-transfer regime, and the IO-ITO|H_2ase electrode exhibited high current densities for proton reduction (>400 μA cm^{-2}) and E_{onset} of −0.35 V versus SHE (pH 6.5, N_2 atmosphere)[3]. Comparison of the voltammetric responses of IO-TiO_2|dpp|P_{Os}–PSII and IO-ITO|H_2ase measured individually (Supplementary Fig. 15) indicated that E_{onset} of the anodic (−0.50 V versus SHE) and cathodic (−0.35 V versus SHE) current responses overlap by approximately 0.15 V (refs [42,44]). Thus, a two-electrode PEC cell that consists of the two enzyme-modified electrodes should be capable of bias-free solar-driven water splitting, assuming only minor resistive solution/membrane losses[45]. A comparison

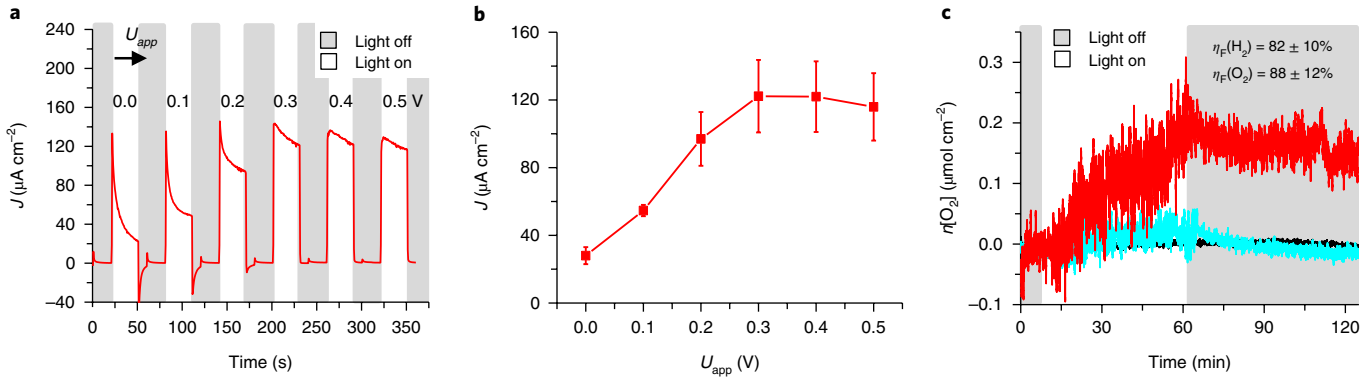

Fig. 4 | Overall water splitting in semi-artificial PEC cell. a, Chronoamperometry (0.1 V voltage steps with 30 s dark and 30 s light cycles) of the two-electrode IO-TiO_2|dpp|P_{Os}–PSII || IO-ITO|H_2ase cell. The applied voltage (U_{app}) values are shown above the peaks. **b**, Photocurrent density as a function of U_{app} based on stepped-voltage ($\Delta U_{app} = 0.1$ V) chronoamperometry measurements for IO-TiO_2|dpp|P_{Os}–PSII || IO-ITO|H_2ase determined in **a**. Values of J were taken at the end of illumination (baseline corrected for the background dark current). Error bars correspond to the s.d. ($n = 3$). **c**, Quantification of O_2 evolution ($\eta_F = 88 \pm 12\%$, $n = 6$) of the photoanode after continuous 1 h illumination (AM1.5 G filter, $E_e = 100$ mW cm^{-2}, $\lambda > 420$ nm) with continuous stirring at $U_{app} = 0.3$ V (red). The amount of H_2 ($\eta_F = 82 \pm 10\%$, $n = 6$) was quantified by gas chromatography analysis. Control experiments in the absence of PSII (blue) and without irradiation (black) are also shown. Conditions: PSII electrolyte solution, pH = 6.5, $T = 25$ °C, continuous stirring, N_2 atmosphere.

of the absolute currents indicates that IO-TiO_2|dpp|P_{Os}–PSII should primarily limit the current response when wired to IO-ITO|H_2ase.

A semi-artificial PEC device was therefore assembled that consisted of an IO-TiO_2|dpp|P_{Os}–PSII photoanode connected to a IO-ITO|H_2ase cathode separated by a glass frit membrane in a two-electrode, two-compartment cell. Figure 4 demonstrates the ability of the system to achieve bias-free solar-driven water splitting. Chronoamperometry measurements with longer irradiation times (Fig. 4a) were performed to minimize the charging effects below an applied voltage (U_{app}) of 0 V. At more positive voltages, the charging effects decreased and photocurrent responses stabilized. On irradiation with ultraviolet-filtered simulated solar light, a current density of $28 \pm 5\,\mu A\,cm^{-2}$ was achieved at $U_{app} = 0$ V (Fig. 4b). Voltage independent steady-state photocurrents ($122 \pm 21\,\mu A\,cm^{-2}$) were reached at $U_{app} = 0.3$ V. The photocurrent magnitudes were similar to those of a two-electrode system with a Pt cathode instead of an IO-ITO|H_2ase (Supplementary Fig. 16), consistent with photocurrent limitation by IO-TiO_2|dpp|P_{Os}–PSII. A two-electrode system with an IO-TiO_2|H_2ase cathode was also assembled and exhibited a similar behaviour, albeit with less charging due to the matched Fermi levels of IO-TiO_2 (Supplementary Fig. 17).

The overall water splitting with the IO-TiO_2|dpp|P_{Os}–PSII || IO-ITO|H_2ase PEC cell was studied at $U_{app} = 0.0$ and 0.3 V (Supplementary Fig. 18a). At zero bias ($U_{app} = 0$ V), the initial photocurrent decayed from $130\,\mu A\,cm^{-2}$ to $5\,\mu A\,cm^{-2}$ after one hour of irradiation, which led to an average half-life time ($\tau_{1/2}$) of 6.5 minutes. At $U_{app} = 0.3$ V, the photocurrent decayed from $140\,\mu A\,cm^{-2}$ to $15\,\mu A\,cm^{-2}$ after one hour of irradiation with a $\tau_{1/2}$ of ~8 min. These lifetimes are similar to those of previously reported PSII-based photoanodes[3,4], and are consistent with the stability of PSII in vivo ($\tau_{1/2}$ of ~20 minutes)[9]. The relative stability of the IO-TiO_2|dpp|P_{Os}–PSII system can be attributed to the efficient electron transfer through TiO_2–dpp–P_{Os}–PSII, the physical stabilization of PSII by the polymer and the reduced accumulation of excited states in chlorophyll *a* within PSII[46]. However, it is important to emphasize that the current hybrid enzyme system is a proof-of-concept device, and its practical applicability is intrinsically limited by the photodegradation pathways of PSII in vitro.

After one hour of continuous light irradiation at $U_{app} = 0.0$ V, H_2 was detected ($0.06\,\mu mol\,H_2\,cm^{-2}$) with a Faradaic efficiency (η_F) of 76%, but a reliable O_2 analysis was prevented by the detection limit of the apparatus. At $U_{app} = 0.3$ V, O_2 and H_2 were quantified (Fig. 4c) with $\eta_F = 88 \pm 12\%$ and $82 \pm 10\%$, respectively (Supplementary Table 1), and a solar-to-hydrogen conversion efficiency of $0.14 \pm 0.02\%$ was obtained[47]. A PSII-based turnover frequency of $2.5 \pm 0.3\,mol\,O_2\,(mol\ PSII)^{-1}\,s^{-1}$ was calculated based on the quantified O_2 and PSII[3,4]. Previously, similar η_F values were reported for benchmark PSII-photoanodes, diffusional-mediated IO-ITO|PSII[3] and IO-ITO|P_{Os}–PSII[4], but they required a significantly higher driving force ($U_{app} = 0.9$ V and $E_{app} = 0.5$ V versus SHE, respectively). Negligible photocurrents were detected in the control experiments (Supplementary Fig. 18b and Supplementary Table 1). O_2 evolution was also confirmed using a rotating ring-disc electrode (RRDE) set-up (Supplementary Fig. 19).

Conclusions

The reported enzyme-based tandem PEC system that consists of an IO-TiO_2|dpp|P_{Os}–PSII photoanode connected to a IO-ITO|H_2ase cathode achieves the long-standing goal of a bias-free in vitro system for overall water splitting using PSII (O_2 generation) connected to H_2ase (H_2 generation). This semi-artificial design addresses key limitations in biology as the PEC wiring of PSII to H_2ase via an abiotic dye allows for (1) a panchromatic solar light absorption by using a synthetic green-light absorber (in contrast to non-complementary absorption by PSI), (2) a quantitative use of electrons extracted from PSII for H_2 production (which thereby avoids inefficient metabolic pathways) and (3) separation of H_2 and O_2 gases in separate compartments (as opposed to inhibiting an O_2-sensitive H_2ase).

The tandem system produced H_2 and O_2 from water with high Faradaic efficiencies in a 2:1 ratio and presents an effective strategy to construct biotic–abiotic interfaces. Future work will involve investigating other dyes and replacing TiO_2 with a semiconductor with a more negative CB potential to enhance the driving force for a more efficient catalysis or CO_2 reduction chemistry. Moreover, our study provides a blueprint to advance future semi-artificial systems capable of bias-free solar fuel and chemical synthesis and a toolbox to develop proof-of-concept model systems for solar energy conversion.

Methods

Materials. 2-(*N*-morpholino)ethane sulfonic acid (Alfa Aesar), tetrabutylammonium hydroxide (Sigma Aldrich), $CaCl_2$ (Breckland Scientific), $MgCl_2$ (Fisher Scientific), KCl (Alfa Aesar), KOH (Breckland Scientific), polystyrene (PS) beads (750 nm diameter, 2.6% w/v suspension in H_2O (Polysciences Inc.), TiO_2 nanoparticles (NPs) (Aeroxide P25 TiO_2 NPs, 21 nm diameter, 80/20 anatase/rutile w/w (Evonik Industries)), ITO NPs (<50 nm

diameter (Sigma Aldrich)), FTO-coated glass slides (8 Ω sq^{-1} (Sigma Aldrich)) and Parafilm (Sigma Aldrich) were purchased from commercial suppliers and used without further purification unless otherwise noted. Methanol, absolute ethanol, 2-propanol, dimethyl sulfoxide and THF (high-performance liquid chromatography grade) were purchased from Sigma Aldrich. PSII was isolated from the thermophilic cyanobacterium *T. elongatus* according to a previously reported procedure[35], with an average oxygen-evolving activity of approximately 5,300 μmol O_2 h^{-1} mg^{-1} of chlorophyll *a*. A stock PSII solution that contained 2.6 mg chlorophyll *a* ml^{-1} (83 μM PSII) was stored in a liquid N_2 Dewar. [NiFeSe]-H_2ase from *D. baculatum* was purified using a previously published method[48], with a specific activity of 2,115 μmol H_2 min^{-1} mg^{-1}. Stock solutions of H_2ase (8 μM in 20 mM Tris/HCl buffer, pH 7.0) were stored in 10–20 μl aliquots at −40 °C in an anaerobic glovebox and used immediately after thawing.

Polymer and dye synthesis. P_{Os} (ref. [37]) was synthesized according to previously reported procedures[4]. In brief, an ethanolic solution of *cis*-[$OsCl_2$(bipy)$_2$] and a poly(1-vinylimidazole-co-allylamine) backbone (1/1.65 weight ratio) was stirred for 5 d at 90 °C. P_{Os} was then precipitated by the addition of diethyl ether, collected by centrifugation, washed thoroughly with diethyl ether, and dried under vacuum to obtain a reddish powder. An aqueous solution of P_{Os} (10 mg ml^{-1}) was used in all the experiments. The dpp-based dye was synthesized using a previously reported procedure[27]. Briefly, pseudo-Stobbe condensation of 1-bromo-4-cyanobenzene with diethyl succinate was followed by lactam *N*-alkylation and then desymmetrization of the intermediate via a Suzuki–Miyaura cross-coupling. The phosphonic acid anchoring group was then added via Hirao cross-coupling using diethyl phosphite followed by hydrolysis. RuP[29] was prepared as previously reported. Both dpp and RuP were characterized as previously reported.

Instrumentation. The surface morphology of the electrodes was analysed by SEM (acceleration voltage 5 kV, working distance 5 mm (Philips SFEG XL30)), energy-dispersive X-ray spectroscopy attached to the SEM, STEM (TitanX 60–300) with a HAADF detector (acceleration voltage 300 kV) and powder X-ray diffraction (Empyrean 2 (PANalytics)). A centrifuge (5804 Eppendorf), furnace (ELF 11/14B/301 (Carbolite)) and ultraviolet/ozone cleaner (ProCleaner Plus (BioForce Nanosciences)) were used for the electrode preparation. UV–vis absorption spectra were recorded on an FS5 spectrofluorometer (integrating sphere reflectance mode (Edinburgh Instruments)) and spectrophotometer (Varian Cary 50 (Agilent)) using cuvettes with an optical path length of 1 cm (transmittance mode). With the integrating sphere, the measurement was performed by concentrating the light reflected from the electrode on the detector using a polytetrafluoroethylene-coated sphere (120 mm in diameter). The relative reflectance was measured with respect to the reflectance of the reference standard white board, which was taken to be 100%.

Preparation of IO-TiO_2 electrodes. The IO-TiO_2 electrodes were fabricated according to a method adopted from a previously reported procedure for the synthesis of IO-ITO[3,4]. FTO-coated glass slides (2 × 1 cm) were cleaned by sonication in two 30 min steps in 2-propanol and absolute ethanol. First, to ensure no direct contact of the electroactive components (PSII and P_{Os}) with the FTO layer, it was coated with a layer of mesoporous TiO_2 (mesoTiO_2). TiO_2 NPs (50 mg) were dispersed via sonication for 20 min in a MeOH/water mixture (300 μl, 5:1 v/v). The suspension (10 μl) was deposited onto a 0.50 cm^2 area defined by a Parafilm ring on an FTO slide and doctor bladed to give a 3-μm-thick mesoTiO_2 layer. The IO-TiO_2 layer was then deposited on top of the mesoTiO_2 layer. TiO_2 NPs (30 mg) were dispersed in a water/MeOH mixture (300 μl, 4:1 v/v) via sonication (3 h). The PS bead dispersion (1 ml) was centrifuged (10,000 revolutions per minute (r.p.m.) for 3 min), and the supernatant was removed. The pellet was redispersed in MeOH (1 ml) before being centrifuged again (10,000 r.p.m. for 0.5 min). The supernatant was removed and the TiO_2 NP dispersion was added to the PS pellet. The pellet was dispersed into the solution by sonication (10 min at <10 °C). The resulting PS-TiO_2 NP dispersion was drop cast (5 μl) onto a 0.25 cm^2 area defined by a Parafilm ring on an FTO slide. After evaporation of the solvent, the electrodes were annealed at a 1 °C min^{-1} ramp rate from room temperature to 500 °C and sintered for 20 min to give a 20 μm thick IO-TiO_2 film. The electrodes were allowed to cool to room temperature and cleaned with an ultraviolet/ozone cleaner (15 min) and characterized by SEM and HAADF–STEM, elemental mapping using energy-dispersive X-ray spectroscopy and powder X-ray diffraction (Supplementary Fig. 2).

Preparation of IO-TiO_2|dye electrodes. IO-TiO_2 electrodes with a pore diameter of 750 nm, a 20 μm film thickness and a geometrical surface area of 0.25 cm^2 were used in all the experiments, unless stated otherwise. The IO-TiO_2|dye-modified electrodes were prepared by soaking IO-TiO_2 electrodes in solutions of dpp or RuP (0.15 mM in THF or H_2O, respectively) overnight in the dark. To remove excess dye prior to the enzyme/polymer deposition, the IO-TiO_2|dpp electrodes were rinsed with THF, followed by water and then air dried. Similarly, the IO-TiO_2|RuP electrodes were rinsed with water and air dried.

Preparation of IO-TiO_2|dye|P_{Os}–PSII electrodes. The IO-TiO_2|dye|P_{Os}–PSII electrodes were prepared by depositing a blend of PSII (1 μl and 2.6 mg chlorophyll *a* ml^{-1}) stock solution and P_{Os} (1 μl, 10 mg ml^{-1}) onto the IO-TiO_2|dye electrode (20 μm thick) and incubating the electrodes in the dark for 15 min at room temperature. Prior to the electrochemical studies, the IO-TiO_2|dye|P_{Os}–PSII electrode was rinsed (3 × 500 μl) with the PSII buffer electrolyte solution (composition given below) to remove loosely bound species from the electrode surface.

Determination of PSII, P_{Os} and dye loading on IO-TiO_2. The amount of PSII on the IO-TiO_2 surface was quantified by scratching off the IO-TiO_2 from the FTO glass substrate and washing it with MeOH (500 μl) to extract chlorophyll *a* (which originated from PSII) from the electrode surface into a centrifuge vial. The vial was centrifuged (10,000 r.p.m. for 1 min), and the UV–vis spectrum of the supernatant was recorded (Supplementary Fig. 4b). The band with an absorption maximum of λ_{max} = 665 nm assigned to chlorophyll *a* (ε = 79.95 (chlorophyll *a* mg)$^{-1}$ ml cm^{-1})[49] was used to calculate the amount of PSII monomers[49] assuming 35 chlorophyll *a* molecules per PSII monomer[33]. The Os-complex loading in the P_{Os} was determined by ICP-OES obtained by washing off the P_{Os} from the IO-TiO_2 electrode with aqueous concentrated HNO_3 solution (70 wt%) and measuring the concentration of the Os metal ions relative to the Os ICP standard (1 mg Os ml^{-1} in 20% HCl (Ricca Chemical)). The dpp/RuP loadings were quantified by scratching off the IO-TiO_2|dye from the glass substrate and washing with tetrabutylammonium hydroxide (0.1 M) in MeOH (500 μl) to extract the dye from the electrode surface into a centrifuge vial. The vial was centrifuged (10,000 r.p.m. for 1 min) and the UV–vis spectrum of the supernatant was recorded (Supplementary Fig. 4a). The amount of dye desorbed into the solution was estimated using the Beer–Lambert Law (Supplementary Fig. 4c,d).

Preparation of IO-ITO|H_2ase electrodes. [NiFeSe]-H_2ase was immobilized on ozone-cleaned IO-ITO electrodes (20 μm film thickness, geometrical surface area, A = 0.25 cm^2) by depositing the enzyme solution (5 μl) on the electrode surface, followed by incubation for approximately 5 min. The loading of [NiFeSe]-H_2ase (40 pmol) was adjusted to the electrode thickness, as reported previously[3].

PF-PEC measurements. Chronoamperometry and cyclic voltammetry measurements were performed using an Ivium Compactstat potentiostat and a gas-tight two-compartment glass cell with a water jacket for temperature control (T = 25 °C). A three-electrode set-up was employed with an IO-TiO_2 (or IO-ITO) working electrode, a Ag/AgCl (3 M KCl) reference electrode and a Pt wire counter electrode separated by a glass frit in another compartment. The cell was filled with a PSII electrolyte solution (12 ml, pH 6.5) that consisted of $CaCl_2$ (20 mM), $MgCl_2$ (15 mM) and KCl (50 mM). All the current densities are reported with respect to the geometrical surface area of the electrodes (μA cm^{-2}) . Experimentally measured potentials are reported versus SHE using the conversion $E_{SHE} = E_{Ag/AgCl} + 0.197$ V (25 °C).

Bias-free PEC overall water splitting and O_2 and H_2 quantification were studied using a two-electrode configuration with an IO-TiO_2 photoanode that contained PSII and an IO-ITO|H_2ase cathode. In all the experiments that involved the IO-ITO|H_2ase cathode, 2-(*N*-morpholino)ethane sulfonic acid (40 mM) was added to the PSII electrolyte solution as it was found to retain the H_2ase electroactivity and only caused negligible photocurrents from 2-(*N*-morpholino)ethane sulfonic acid oxidation.

PEC experiments were performed using a Xe lamp (150 W (Newport)) solar light simulator (E_e = 100 mW cm^{-2}, AM 1.5 G filter, λ > 420 nm filter (LOT Quantum Design)). Action spectra were recorded with a Xe lamp (300 W (Newport)) solar light simulator (LOT Quantum Design) coupled to a monochromator (MSH300 (LOT Quantum Design)). For the dual excitation experiments, an Ivium ModuLight light-emitting diode module (λ = 460/523/660 nm; 4 mW cm^{-2}) was used as a second light source. Light intensity was measured as a function of wavelength with a thermal sensor (S302C (Thorlabs)) and power meter console (PM100D (Thorlabs)).

IO–TiO_2|dye|P_{Os}–PSII electrodes were exposed to dark and light cycles in the PF-PEC measurements. To avoid an overestimation of the photocurrent, the photocurrent response was defined as the baseline-corrected (dark-current subtracted) photocurrent peak shoulder edge after light exposure[9]. Action spectra were corrected to equal the photon flux at each wavelength and normalized (taking the peak at 500 nm as unity). Error bars are ±s.d. of the sample estimated from at least three experiments. All the data processing was performed using OriginPro 9.1 software.

RRDE experiments were performed using a Ag/AgCl (3 M KCl) reference and glassy carbon counter electrodes. The disk/ring apparatus was embedded in a cylindrical polyether ether ketone housing. A Pt ring electrode surrounded a glassy carbon disk electrode on which a mesoTiO_2 layer was deposited prior to depositing additional components (dpp, P_{Os} and PSII). The electrodes were placed in a single-compartment cell under continuous purging with N_2. The ring/disk electrode was rotated at 400 r.p.m. for the O_2 evolution measurements and the collection efficiency of the ring electrode was calibrated under conditions similar to those of the experiment (Supplementary Fig. 19).

Product analysis. Quantification of O_2 was performed using a fluorescence-based O_2 sensor (Ocean Optics FOSFOR-R probe (Neofox) inside an anaerobic

glovebox (Belle Technology) to avoid the ingress of atmospheric O_2. The probe was placed inside the anodic compartment headspace of a two-compartment cell protected from direct irradiation. The results are reported as the average of six measurements and the background signal was subtracted from all the measurements. The reported O_2 values were corrected for dissolved O_2 using Henry's law ($K_{H(O2)}$ = 769.231 atm mol^{-1} at 25 °C). H_2 was analysed by taking aliquots of the headspace gas (50 µl) after electrolysis and quantified using gas chromatography (carrier gas N_2, flow rate 0.7 ml min^{-1}, molecular sieve column, thermal conductivity detector (Agilent 7890)). Calibration runs were performed to quantify the volume of H_2 evolved. The reported Faradaic efficiencies were corrected by subtracting the dpp dye background current estimated from control experiments from the experimental data.

Data availability. The data that support the presented plots within this paper and other findings of this study are available at the University of Cambridge data repository with the identifier https://doi.org/10.17863/CAM.25834.

Received: 25 May 2018; Accepted: 26 July 2018;
Published online: 03 September 2018

References

1. Sakimoto, K. K., Wong, A. B. & Yang, P. Self-photosensitization of nonphotosynthetic bacteria for solar-to-chemical production. *Science* **351**, 74–77 (2016).
2. Yehezkeli, O. et al. Integrated photosystem II-based photo-bioelectrochemical cells. *Nat. Commun.* **3**, 742 (2012).
3. Mersch, D. et al. Wiring of photosystem II to hydrogenase for photoelectrochemical water-splitting. *J. Am. Chem. Soc.* **137**, 8541–8549 (2015).
4. Sokol, K. P. et al. Rational wiring of photosystem II to hierarchical indium tin oxide electrodes using redox polymers. *Energy Environ. Sci.* **9**, 3698–3709 (2016).
5. Ort, D. R. et al. Redesigning photosynthesis to sustainably meet global food and bioenergy demand. *Proc. Natl Acad. Sci. USA* **112**, 8529–8536 (2015).
6. Tachibana, Y., Vayssieres, L. & Durrant, J. R. Artificial photosynthesis for solar water-splitting. *Nat. Photon.* **6**, 511–518 (2012).
7. Woolerton, T. W., Sheard, S., Chaudhary, Y. S. & Armstrong, F. A. Enzymes and bio-inspired electrocatalysts in solar fuel devices. *Energy Environ. Sci.* **5**, 7470–7490 (2012).
8. Léger, C. & Bertrand, P. Direct electrochemistry of redox enzymes as a tool for mechanistic studies. *Chem. Rev.* **108**, 2379–2438 (2008).
9. Kato, M., Zhang, J. Z., Paul, N. & Reisner, E. Protein film photoelectrochemistry of the water oxidation enzyme photosystem II. *Chem. Soc. Rev.* **43**, 6485–6497 (2014).
10. Bard, A. J. & Fox, M. A. Artificial photosynthesis: solar splitting of water to hydrogen and oxygen. *Acc. Chem. Res.* **28**, 141–145 (1995).
11. Govindjee, Shevela, D. & Björn, L. O. Evolution of the Z-scheme of photosynthesis: a perspective. *Photosynth. Res.* **133**, 5–15 (2017).
12. Barber, J. & Tran, P. D. From natural to artificial photosynthesis. *J. R. Soc. Interface* **10**, 20120984 (2013).
13. Khetkorn, W. et al. Microalgal hydrogen production—a review. *Bioresource Technol.* **243**, 1194–1206 (2017).
14. Kruse, O., Rupprecht, J., Mussgnug, J. H., Dismukes, G. C. & Hankamer, B. Photosynthesis: a blueprint for solar energy capture and biohydrogen production technologies. *Photochem. Photobiol. Sci.* **4**, 957–969 (2005).
15. Michel, H. The nonsense of biofuels. *Angew. Chem. Int. Ed.* **51**, 2516–2518 (2012).
16. Esper, B., Badura, A. & Rögner, M. Photosynthesis as a power supply for (bio-)hydrogen production. *Trends Plant Sci.* **11**, 543–549 (2006).
17. Hu, S., Xiang, C., Haussener, S., Berger, A. D. & Lewis, N. S. An analysis of the optimal band gaps of light absorbers in integrated tandem photoelectrochemical water-splitting systems. *Energy Environ. Sci.* **6**, 2984–2993 (2013).
18. Kothe, T. et al. Combination of a photosystem I-based photocathode and a photosystem II-based photoanode to a Z-scheme mimic for biophotovoltaic applications. *Angew. Chem. Int. Ed.* **52**, 14233–14236 (2013).
19. Hartmann, V. et al. Redox hydrogels with adjusted redox potential for improved efficiency in Z-scheme inspired biophotovoltaic cells. *Phys. Chem. Chem. Phys.* **16**, 11936–11941 (2014).
20. Kim, Y. et al. Hybrid Z-scheme using photosystem I and $BiVO_4$ for hydrogen production. *Adv. Funct. Mater.* **25**, 2369–2377 (2015).
21. Rao, K. K. et al. Photoelectrochemical responses of photosystem II particles immobilized on dye-derivatized TiO_2 films. *J. Photochem. Photobiol. B* **5**, 379–389 (1990).
22. Wang, W. et al. Spatially separated photosystem II and a silicon photoelectrochemical cell for overall water splitting: a natural–artificial photosynthetic hybrid. *Angew. Chem. Int. Ed.* **55**, 9229–9233 (2016).
23. Pinhassi, R. I. et al. Hybrid bio-photo-electro-chemical cells for solar water splitting. *Nat. Commun.* **7**, 12552 (2016).
24. O'Regan, B. & Grätzel, M. A low-cost, high-efficiency solar cell based on dye-sensitised colloidal TiO_2 films. *Nature* **353**, 737–740 (1991).
25. Xu, P., McCool, N. S. & Mallouk, T. E. Water splitting dye-sensitized solar cells. *Nano Today* **14**, 42–58 (2017).
26. Warnan, J. et al. A compact diketopyrrolopyrrole dye as efficient sensitizer in titanium dioxide dye-sensitized solar cells. *J. Photochem. Photobiol. A* **226**, 9–15 (2011).
27. Warnan, J. et al. Solar H_2 evolution in water with modified diketopyrrolopyrrole dyes immobilised on molecular Co and Ni catalyst–TiO_2 hybrids. *Chem. Sci.* **8**, 3070–3079 (2017).
28. Muresan, N. M., Willkomm, J., Mersch, D., Vaynzof, Y. & Reisner, E. Immobilization of a molecular cobaloxime catalyst for hydrogen evolution on a mesoporous metal oxide electrode. *Angew. Chem. Int. Ed.* **51**, 12749–12753 (2012).
29. Lakadamyali, F., Reynal, A., Kato, M., Durrant, J. R. & Reisner, E. Electron transfer in dye-sensitised semiconductors modified with molecular cobalt catalysts: photoreduction of aqueous protons. *Chem. Eur. J.* **18**, 15464–15475 (2012).
30. Knauf, R. R., Brennaman, M. K., Alibabaei, L., Norris, M. R. & Dempsey, J. L. Revealing the relationship between semiconductor electronic structure and electron transfer dynamics at metal oxide−chromophore interfaces. *J. Phys. Chem. C* **117**, 25259–25268 (2013).
31. Li, F. et al. Immobilizing Ru(bda) catalyst on a photoanode via electrochemical polymerization for light-driven water splitting. *ACS Catal.* **5**, 3786–3790 (2015).
32. Willkomm, J. et al. Dye-sensitised semiconductors modified with molecular catalysts for light-driven H_2 production. *Chem. Soc. Rev.* **45**, 9–23 (2016).
33. Umena, Y., Kawakami, K., Shen, J.-R. & Kamiya, N. Crystal structure of oxygen-evolving photosystem II at a resolution of 1.9 Å. *Nature* **473**, 55–60 (2011).
34. Rapatskiy, L. et al. Detection of the water-binding sites of the oxygen-evolving complex of photosystem II using W-band ^{17}O electron−electron double resonance-detected NMR spectroscopy. *J. Am. Chem. Soc.* **134**, 16619–16634 (2012).
35. Kuhl, H. et al. Towards structural determination of the water-splitting enzyme: purification, crystallization, and preliminary crystallographic studies of photosystem II from a thermophilic cyanobacterium. *J. Biol. Chem.* **275**, 20652–20659 (2000).
36. Kern, J. et al. Purification, characterisation and crystallisation of photosystem II from *Thermosynechococcus elongatus* cultivated in a new type of photobioreactor. *Biochim. Biophys. Acta Bioenerg.* **1706**, 147–157 (2005).
37. Badura, A. et al. Photo-induced electron transfer between photosystem II via cross-linked redox hydrogels. *Electroanalysis* **20**, 1043–1047 (2008).
38. Senge, M. O., Ryan, A. A., Letchford, K. A., MacGowan, S. A. & Mielke, T. Chlorophylls, symmetry, chirality, and photosynthesis. *Symmetry* **6**, 781–843 (2014).
39. Beranek, R. (Photo)electrochemical methods for the determination of the band edge positions of TiO_2-based nanomaterials. *Adv. Phys. Chem.* **2011**, 80–83 (2011).
40. Zhang, J. Z. et al. Competing charge transfer pathways at the photosystem II–electrode interface. *Nat. Chem. Biol.* **12**, 1046–1052 (2016).
41. Razeghifard, R. & Wydrzynski, T. J. *Artificial Photosynthesis: From Basic Biology to Industrial Application* (Wiley, Hoboken, 2007).
42. Reisner, E., Powell, D. J., Cavazza, C., Fontecilla-Camps, J. C. & Armstrong, F. A. Visible light-driven H_2 production by hydrogenases attached to dye-sensitized TiO_2 nanoparticles. *J. Am. Chem. Soc.* **131**, 18457–18466 (2009).
43. Wombwell, C., Caputo, C. A. & Reisner, E. [NiFeSe]-hydrogenase chemistry. *Acc. Chem. Res.* **48**, 2858–2865 (2015).
44. Hambourger, M. et al. [FeFe]-hydrogenase-catalyzed H_2 production in a photoelectrochemical biofuel cell. *J. Am. Chem. Soc.* **130**, 2015–2022 (2008).
45. Coridan, R. H. et al. Methods for comparing the performance of energy-conversion systems for use in solar fuels and solar electricity generation. *Energy Environ. Sci.* **8**, 2886–2901 (2015).
46. Cai, P. et al. Co-assembly of photosystem II/reduced graphene oxide multilayered biohybrid films for enhanced photocurrent. *Nanoscale* **7**, 10908–10911 (2015).
47. Dotan, H., Mathews, N., Hisatomi, T., Grätzel, M. & Rothschild, A. On the solar to hydrogen conversion efficiency of photoelectrodes for water splitting. *J. Phys. Chem. Lett.* **5**, 3330–3334 (2014).
48. Hatchikian, E. C., Bruschi, M. & Le Gall, J. Characterisation of the periplasmic hydrogenase from *Desulfovibrio gigas*. *Biochem. Biophys. Res. Commun.* **82**, 451–461 (1978).
49. Porra, R. J., Thompson, W. A. & Kriedemann, P. E. Determination of accurate extinction coefficients and simultaneous equations for assaying chlorophylls *a* and *b* extracted with four different solvents: verification of the concentration of chlorophyll standards by atomic absorption spectroscopy. *Biochim. Biophys. Acta Bioenerg.* **975**, 384–394 (1989).

Acknowledgements

This work was supported by an ERC Consolidator Grant MatEnSAP (682833), the UK Engineering and Physical Sciences Research Council (EP/L015978/1 and EP/G037221/1, nanoDTC and a DTA studentship), the Christian Doppler Research Association, the OMV Group and a Royal Society Newton International Fellowship (NF160054), the Cluster of Excellence RESOLV (EXC 1069) funded by the Deutsche Forschungsgemeinschaft and the European Union's Horizon 2020 MSCA ITN-EJD 764920 PHOTOBIOCAT. The HAADF–STEM was carried out at the National Center of Electron Microscopy (NCEM), which is supported by the Office of Science, Office of Basic Energy Sciences of the US Department of Energy under Contract no. DE-AC02-05CH11231. Work at the Molecular Foundry was supported by the Office of Science, Office of Basic Energy Sciences of the US Department of Energy under Contract no. DE-AC02-05CH11231. We thank J. Fontecilla-Camps and C. Cavazza for providing the H_2ase enzyme, V. Hartmann for his contribution to the PSII preparation and N. Plumeré, C. Creissen, S. Kalathil and N. Heidary for valuable discussions.

Author contributions

K.P.S., W.E.R., J.Z.Z. and E.R. conceived the research. K.P.S. prepared and characterized the electrodes and performed the electrochemical experiments. W.E.R. helped with the experiment design and supported the electrochemical experiments. J.W. synthesized the dpp dye. N.K. carried out the HAADF–STEM and RRDE measurements. M.M.N. provided the PSII samples. A.R. synthesized the P_{Os} polymer. K.P.S., W.E.R., N.K., J.Z.Z. and E.R. analysed the data. All the authors contributed to the creation of the manuscript. E.R. supervised the work.

Competing interests

The authors declare no competing interests.

Additional information

Supplementary information is available for this paper at https://doi.org/10.1038/s41560-018-0232-y.

Reprints and permissions information is available at www.nature.com/reprints.

Correspondence and requests for materials should be addressed to E.R.

Publisher's note: Springer Nature remains neutral with regard to jurisdictional claims in published maps and institutional affiliations.